European Journal of Pharmaceutics and Biopharmaceutics 74 (2010) 14–20

Contents lists available at ScienceDirect

European Journal of Pharmaceutics and Biopharmaceutics

journal homepage: www.elsevier.com/locate/ejpb

Research paper

FTIR microscopy and confocal Raman microscopy for studying lateral drug diffusion from a semisolid formulation

B. Gotter [a,*], W. Faubel [b], R.H.H. Neubert [a,c]

[a] Institute of Pharmacy, Martin Luther University, Halle/Saale, Germany
[b] Institute of Functional Interfaces, Karlsruhe Research Centre, Karlsruhe, Germany
[c] Institute of Applied Dermatopharmacy, Halle/Saale, Germany

ARTICLE INFO

Article history:
Received 28 November 2008
Accepted in revised form 10 July 2009
Available online 15 July 2009

Keywords:
FTIR microscopy
Confocal Raman microscopy
Drug diffusion
Semisolid formulations
Non-invasive
Imaging
Mapping
3D mapping

ABSTRACT

Fourier transform infrared (FTIR) microscopy was applied to obtain information on lateral drug diffusion of dithranol in artificial acceptor membranes. Lateral (2D) drug distribution into an artificial membrane was investigated on an area of 300 μm × 1000 μm with a lateral resolution of 25 μm × 25 μm by integrating a specific IR band located at 1430 cm^{-1}. The concentration profiles show a heterogeneous distribution of dithranol particles resulting in non-uniform drug diffusion. Use of the FTIR microscope either in the transmission or in the reflection mode was restricted to a thickness of the DDC membrane <15 μm. The third dimension (depth profile) was analysed by means of confocal Raman microscopy (CRM). In an artificial membrane, the depth range from a minimum of 1.5 μm up to a maximum of 49 μm was analysed for dithranol distribution.

1. Introduction

Infrared (IR) and Raman spectra, which are complementary to each other, provide descriptions of molecular vibrational transitions of the atoms of a compound. Therefore, both techniques are also referred to as vibrational spectroscopy. Vibrational spectroscopy is widely used in pharmaceutical research and technology and quality inspection as well as in quantification.

The infrared and Raman spectroscopy techniques developed in the past decades gave rise to a number of new applications. FTIR-ATR (Fourier transform infrared attenuated total reflection) spectroscopy, FTIR-PAS (Fourier transform infrared photoacoustic spectroscopy) and FTIR-RAS (Fourier transform infrared reflection–absorption spectroscopy) as well as FT-Raman (Fourier transform Raman) spectroscopy are to be mentioned in this context. FTIR-ATR has become a standard method in the field of real-time drug penetration studies in membranes and for the investigation of drug release from pharmaceutical formulations. It was successfully demonstrated that the FTIR-ATR technique is capable of providing data on the release process of drugs in semisolid formulations [1]. Another development for the investigation of the drug diffusion process consists in the use of an FTIR-ATR cell for non-invasive real-time measurements. The diffusion of water through an artificial polyethylene glycol/polydimethylsiloxane membrane was studied. Additionally, the diffusion of urea in the human stratum corneum was analysed [2]. FTIR-PAS supplies chemical information even about opaque samples. To study drug delivery from pharmaceutical formulations and the penetration of compounds into skin or membranes, the phase modulation technique was employed frequently [3]. It allows to reach certain ranges of the sample depths of up to 50 μm. For the measurement of thin films, the IRRAS technique is applied. It yields spectral information on layers down to a thickness of 1 nm [4]. Since FT-Raman spectroscopy is sensitive to conformational order of molecules, it is often applied to characterise compounds with respect to their molecular structures e.g. the structure of stratum corneum lipids [5].

Investigation of inhomogeneous systems requires the composition of specific molecules or functional groups in a certain sample to be displayed. This information can be obtained by means of vibrational spectroscopic imaging techniques. Imaging advantages partly result from the investigator's ability to efficiently process and generate a complex two-dimensional spatial representation of a sample in terms of a variety of spectrally related molecular parameters. The use of imaging for biological purposes has increased rapidly. Chemical images of single cells, even human cells, were recorded and showed the protein distribution, the

* Corresponding author. Institute of Pharmacy, Martin Luther University, 06114 Halle/Saale, Germany. Tel.: +49 3455525214.
E-mail address: bernhard.gotter@pharmazie.uni-halle.de (B. Gotter).

0939-6411/$ - see front matter © 2009 Elsevier B.V. All rights reserved.
doi:10.1016/j.ejpb.2009.07.006

localisation of the nucleus, organelles, and the membrane [6–8]. Application of Raman microspectroscopy and imaging to study chemical heterogeneity of emulsion systems was reported too [9]. Since confocal Raman microscopy provides depth-resolved measurements, this technique was frequently used to observe drug penetration into the human skin [10,11] and to study the hydration levels of certain layers of the human epidermis [12,13]. Recent developments in the field of Raman technique are the CARS (coherent anti-Stokes Raman scattering) microscopy [14] and the stimulated Raman scattering (SRS) microscopy. Freudiger et al. reported a three-dimensional multiphoton vibrational imaging technique based on stimulated Raman scattering (SRS). The sensitivity of SRS imaging is significantly higher than that of spontaneous Raman microscopy, and SRS can be applied to monitor drug delivery and for skin imaging [15].

The use of FTIR imaging as an analytical tool for the characterisation of drug delivery systems was demonstrated by C.A. Coutts-Lendon et al. [16]. In their study, the delivery characteristics of the drug, testosterone, suspended in a poly(ethylene oxide) matrix were observed using this technique. Kazarian et al. applied FTIR–ATR imaging for the "chemical photography" of the release process of polymer/drug formulations [17]. This is to name only a few publications that deal with spectroscopic methods for the investigation of skin composition, skin hydration, and skin penetration and illustrate the benefits of spectroscopy and in particular of spectroscopic imaging in this field of science.

In the following work, the application of FTIR imaging for investigating the lateral penetration of the model drug dithranol (DI) within an artificial membrane [18] will be discussed. In-depth investigation of the penetration process by measuring the third dimension (sample depth) using confocal Raman imaging will be presented. The system applied for this purpose is an artificial acceptor membrane (DDC membrane) and a formulation of white soft paraffin containing the anti-psoriatic drug dithranol (DI). The DDC membrane acts like a lipophilic acceptor and does not quite match real conditions of the human skin. Nevertheless, this system allows for assessing physicochemical properties of drugs and drug delivery from various vehicles.

2. Experimental

2.1. Introduction to imaging techniques

Before describing the experiments in detail, it appears reasonable to recall some basic theory. Electromagnetic radiation of the infrared region is absorbed by matter when its frequency corresponds to the frequency of a molecular vibration, which is able to alter the dipole moment of the molecule. An IR spectrum is obtained by passing infrared radiation through a sample and by determining the absorbed fraction of the incident radiation. Detection of Raman scattering radiation results from a laser-induced excitation of a sample. There are several kinds of light scattering. While Rayleigh scattering leads to no change in the wavelength of individual photons, the Raman effect leads to a change in energy of some photons due to inelastic collision of incident light and molecules. Depending on the energetic state of the vibration interacting with the photon, the scattered radiation may lose energy. This case is referred to as Stokes Raman scattering. If the created photon is of higher energy, the anti-Stokes spectrum will be produced. Recording of the Stokes Raman spectrum is sufficient in most applications. The basic theory of infrared spectroscopy [19–23] as well as of Raman spectroscopy [21,24–26] is discussed in detail in various publications.

Both infrared and Raman spectroscopy are contactless, non-destructive, and minimally invasive or even non-invasive technologies, which provide vast chemical information about the subject of interest. The combination of IR and Raman spectrometers with microscopes turned out to be a great leap forward in the field of vibrational spectroscopy in life sciences [27,28]. It does not only supply chemical information on bulk samples, but also supply a photography of the sample, from which chemical information of high spatial resolution can be derived for each point. Introduction of vibrational microscopy made chemical visualisation possible. In its most basic form, chemical visualisation data can be acquired in the following ways: point mapping with a single-element detector or global imaging with an array detector (Fig. 1). In the first case, single measuring points are visualised by moving the sample in the focused laser or infrared beam with a motorised x–y stage. At each position, a complete spectrum is recorded using a standard spectrograph with a detector. The output is a vibrational spectrum corresponding to each spatial location. Then, chemical information can be interlinked by data processing. In contrast to this, a wide area of the sample is subject to Raman excitation or infrared scanning, if a defocused beam is applied. When using an FPA (focal plane array) or CCD (charge coupled device) array detector, a series of images is recorded as a function of the wave number [20]. Many of the methods employed for infrared and Raman imaging collect the radiation by a microscope objective and guide it to a tuneable filter for wavelength selection. The filtered radiation is collected by the array detectors mentioned above, which provide the two spatial dimensions. The third dimension is obtained by tuning the filter.

To sum up, two categories of imaging techniques are distinguished: "direct imaging" and "series imaging" methods. The direct imaging technique results in the immediate production of a complete two-dimensional image at a chosen wavelength, which is characteristic of a molecular compound within the fully illuminated specimen. On the other hand, series imaging or mapping techniques require image reconstruction, which is achieved by scanning the sample [29].

2.2. Raman measurements

Raman series imaging experiments were carried out with the Raman microscope Senterra (Bruker Optics, Ettlingen, Germany)

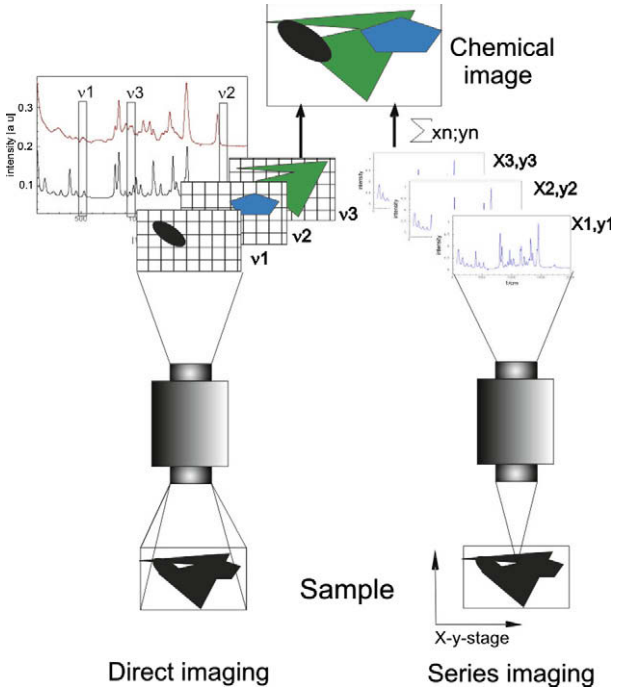

Fig. 1. Options for chemical imaging using vibrational spectroscopy.

for depth-resolved measurements. As excitation source, a diode laser (785 nm, 100 mW) was employed. The excitation beam as well as the Raman backscattering radiation was guided through a 50× objective (NA = 0.75). By means of a confocal diaphragm of 50 μm diameter, the Raman scattering radiation emanating from the focal plane only was permitted to reach the detector's CCD camera. A typical integration time for recording the Raman spectra was 90 s on the average. The spectral resolution was 4 cm^{-1} in the spectral range from 75 cm^{-1} to 1535 cm^{-1}. This spectral region was chosen, since the most intensive Raman bands of dithranol were located here. The experimental set-up was composed of a sample holder that contained a gap, which served as a reservoir for the semisolid pharmaceutical formulation, which was a 5% suspension of the anti-psoriatic drug dithranol in white soft paraffin. Above this arrangement, a DDC membrane [28] made of collodion and 4% dodecanol was positioned. Its average thickness amounted to 31 μm and the index of refraction was $n_D^{20} = 1.465$ (measured by means of an Abbe refractometer). In order to observe the distribution of dithranol in the membrane, a measuring field of 45 μm × 210 μm was arranged. It contained 16 points (resolution: 15 μm × 70 μm). The confocal microscope allowed for measurements in three layers, namely, on the surface of the membrane, at an adjusted depth of 10 μm, and at a depth of 20 μm (Fig. 2). Consequently, a single measurement consisted of 48 spectra representing an observed cubic space of 0.189 mm^3 of the DDC membrane and a spatial resolution of 15 μm × 70 μm × 10 μm ($x/y/z$).

Mapping of a single layer took 30 min, resulting in a total acquisition time of more than 90 min. For analysis, a pre-treatment procedure was applied to all spectra using the OPUS software (version 6.5 Bruker Optics, Ettlingen, Germany). The treatment comprised a baseline correction procedure with subsequent smoothing of the spectral data. Finally, the spectra were normalised to the band at 848 cm^{-1}, which can be assigned to the DDC membrane (Fig. 5).

2.3. FTIR measurements

The direct IR imaging experiment was accomplished using the infrared microscope HYPERION 3000. For series IR imaging, the FTIR spectrometer IFS66 was coupled with the IR-scope II (Bruker Optics, Ettlingen, Germany). In the case of direct imaging experiment with HYPERION 3000, the signal-to-noise ratio of the bands of interest was too low to allow for an interpretation of the data (data not shown). Due to the lower sensitivity of direct imaging, the experiments were carried out by using the mapping or series imaging mode. The spectra in the range of 680–4000 cm^{-1} were acquired with 20 scans at a resolution of 2 cm^{-1}. The DDC membrane thickness was restricted to less than 15 μm. When using thicker membranes, the absorbance of the infrared radiation would have been too high in this measuring mode (transmission). The experimental set-up is shown in Fig. 3. The sample used was a 10% suspension of dithranol in white soft paraffin. The DDC membrane was used as an acceptor membrane.

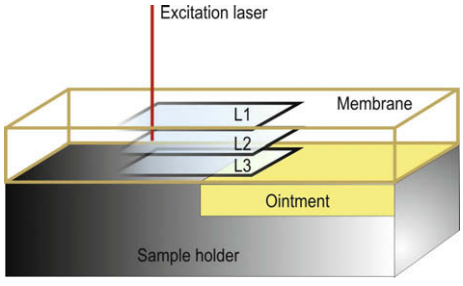

Fig. 2. Experimental scheme for the series imaging of the diffusion of dithranol using a Raman microscope. Imaging was performed in three layers of different depths in the DDC membrane L1, L2, and L3.

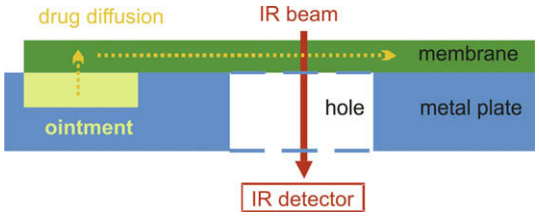

Fig. 3. Experimental scheme for the series imaging of the diffusion of dithranol in a DDC membrane using an IR microscope in the transmission mode.

3. Results and discussion

The system used in our investigations has already been under research for several years by means of various spectroscopic techniques [30–32]. The artificial membrane serves as a skin model showing the properties of a lipophilic acceptor system, while the formulation represents the donor. Since dithranol is a substance with pronounced lipophilic properties, it is highly soluble in the membrane mentioned. The partition coefficient of dithranol between the DDC membrane and white soft paraffin was defined by Hanh to range between 1.37 and 2.07. The delivery of dithranol from the formulation used into the membrane was studied elsewhere and is known to occur [33]. This well-known arrangement is considered appropriate for investigations that use imaging techniques.

The IR imaging results were taken from a study to elucidate the potential use of the FTIR microscope (mapping and imaging techniques) for determining the lateral penetration of a drug from semisolid formulations into artificial lipid membranes [18]. An area of 300 μm × 1000 μm of the membrane was used to determine drug distribution. The whole area was measured for 2.5 h with a lateral resolution of 25 μm × 25 μm. DI exhibits a strong IR band at 1446 cm^{-1}, which is derived from ring stretching vibrations, similar to the band in anthracenes. By integration of the drug's IR band (1398–1472 cm^{-1}), the concentration distance profile of dithranol in the DDC membrane was generated (Fig. 4). The concentration profiles show that there is a heterogeneous distribution of dithranol particles in the formulation, which results in a non-uniform drug diffusion front in the membrane. However, no changes of drug concentration with depth were obtained by Hanh et al. [18]. In order to obtain more information on deeper layers of the sample, confocal Raman microscopy is a versatile tool and is suitable to overcome the limitations of micro FTIR.

Initially, Raman measurements of the individual components were accomplished. Damages of the samples due to laser radiation such as deformation, ablation or photochemical reactions were not observed. The resulting spectra (Fig. 5) show characteristic bands of the active molecular vibrations of the ingredients. White soft paraffin is a mixture of *n*- and iso-paraffin, which exhibit a typical number of bands, namely, the peak around 1460 cm^{-1} consisting of the $-(CH_2)$ band of the scissoring mode usually found at 1465 cm^{-1} and the asymmetric CH_3 band typically located between 1470 cm^{-1} and 1430 cm^{-1}. The second band of strong intensity is located at 1296 cm^{-1} and can be assigned to the $-(CH_2)_n-$ in-phase twisting mode of asymmetric bending vibrations in *n*-alkanes [34]. These vibrations also occur in the artificial membrane, since collodion and in particular the long-chain alcohol dodecanol are composed of several similar functional groups. In primary and secondary alcohols, the CCO stretching frequencies occur between 800 cm^{-1} and 900 cm^{-1}. The hydroxyl group exists in the long-chained alcohol as well as in the collodion. Furthermore, the nitro

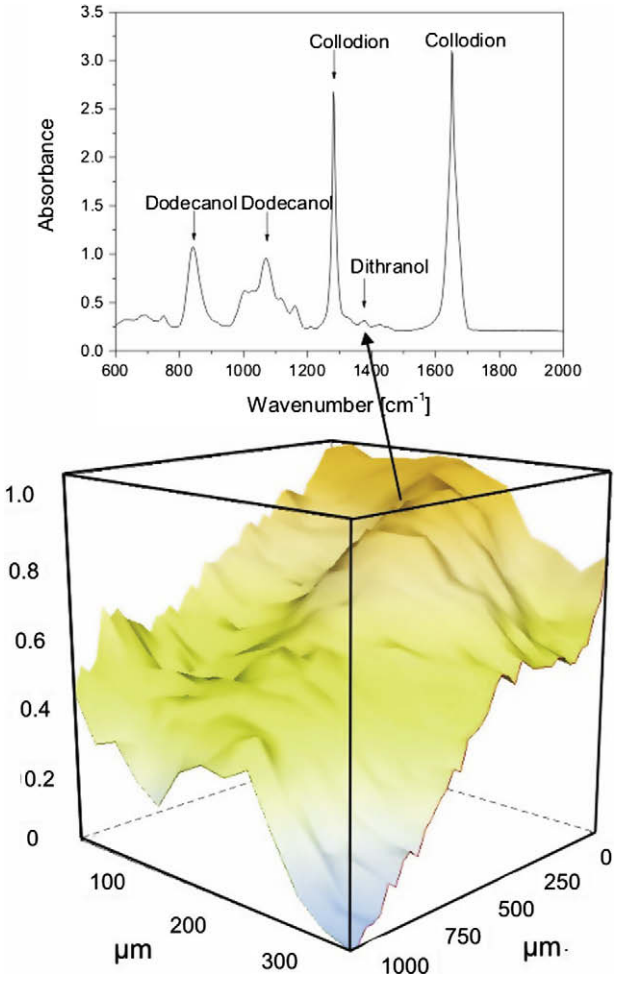

Fig. 4. FTIR mapping of the lateral diffusion of dithranol in a vaseline formulation into a dodecanol–collodion membrane (thickness 12 µm). The *X*-axis and *Y*-axis represent the observed membrane area, and the *Z*-axis indicates the normalised drug amount. The spectrum shows the DDC membrane containing the penetrated drug. For extracting the drug concentration profile, the integrated intensity of the dithranol band in the spectral range of 1398–1472 cm^{-1} was used (taken from [18] with permission of Elsevier).

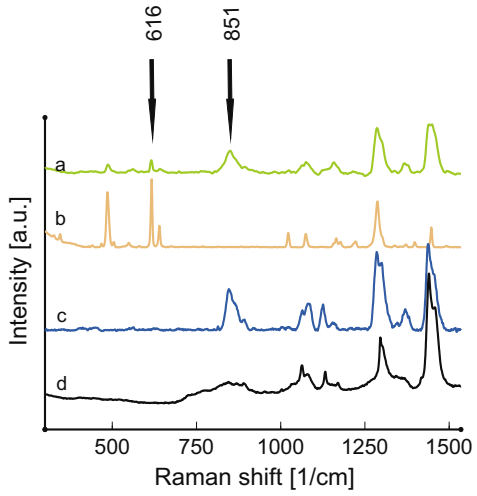

Fig. 5. Raman spectra of the applied compounds: (a) DDC membrane containing traces of dithranol measured during the experiment; (b) pure active ingredient dithranol; (c) DDC membrane measured when experiment was started; and(d) white soft paraffin. The arrows indicate the bands used for determination of the dithranol. The assigned molecular vibrations for 616 cm^{-1} and 851 cm^{-1} are presented in the results part.

group contributes to the intensive signal in this range. The molecular structure of dithranol is composed of anthracene with three hydroxyl groups at positions 1, 8, and 9. The spectrum of dithranol shows two intensive bands between 650 cm^{-1} and 450 cm^{-1}. These signals are probably due to ring deformation modes, which are typically present in condensed mono-substituted benzenes. Considering the spectra of the DDC membrane and paraffin, the dithranol bands are isolated in the spectrum, which makes them suitable means to pursue the diffusion process. Consequently, the band of dithranol at 616 cm^{-1} was integrated to relate the drug amount in the membrane. The spectrum in Fig. 5a was extracted from the mapping experiment. It was recorded 60 h after preparation of the sample arrangement. The bands emanating from the drug are detectable at 616 cm^{-1} and 485 cm^{-1}. In order to observe the distribution of dithranol in the DDC membrane, a measuring field of 45 µm × 215 µm containing 16 points was arranged. Four measuring points were located where the membrane covered the formulation. This area was subjected to measurements at three defined depths by varying the vertical sample position. When measuring in three-dimensions, however, the focus must be below the surface of the sample. The Raman microscope applied was configured with metallurgical objectives and designed to work in air. If this is the case, the tightly convergent laser beam will suffer refraction at the sample/air interface and it becomes difficult to define the correct *z* coordinate.

Everall describes the effect of refraction on the depth resolution of confocal Raman microscopy and found that position and depth of focus increase dramatically when moving deeper into the transparent media. By means of the ray-tracing model, he presents a simple method for evaluating the true localisation and depth of the focus in the sample [35].

$$Z = \Delta \sqrt{\left[m^2 \frac{NA^2(n^2-1)}{1-NA^2} + n^2 \right]} \quad (1)$$

This equation gives the true point of the focus (z) as a function of the apparent focal point (Δ), the refractive index (n) of the medium, and the numerical aperture (NA). The distance across the microscope is normalised in terms of the pupil parameter m; while $m = 0$ corresponds to normal incident rays, $m = 1$ corresponds to rays with the maximum incident angle. Using this analysis, the true position of the measurement layers was calculated (Table 1). The attentive reader would have noticed the divergence between the thickness of the membrane, namely, 31 µm, and the calculated theoretical depth of L3 that ranges from 29 µm to 49 µm. This means that the lowest layer L3 represents a depth range of the membrane, which is not exactly defined. In the case of the region where the holder confines the DDC membrane, it is quite difficult to make a conclusion with regard to the origin of the measured signals. However, no disturbing bands were recorded, and due to reflection and scattering on the holder surface, the collected signals were supposed to originate from a not exactly defined region of the membrane. This section was considered the lowest part with properties of a boundary layer. This means that at places where the membrane covers the ointment, the spectra contain information about the important interface region membrane/formulation.

Table 1
Adjusted and corrected focus positions of L1, L2 and L3, which were calculated by using Eq. (1).

Layer	Apparent depth Δ (µm)	Z_{min} (µm)	Z_{max} (µm)	Focal depth (µm)
L1	1	1.47	2.46	0.99
L2	10	14.65	24.60	9.95
L3	20	29.3	49.2	19.9

Images of the DI distribution of the membrane sections (according experimental scheme shown in Fig. 2) measured as a function of time and depth are given in Fig. 6. The first observation is the heterogeneity of the DI concentration at ointment/sample holder interface, which is characterised by variations of the signal intensities. This suggests that the contact between ointment, sample holder, and the membrane is not equally well all over. This would have to be considered, if diffusion kinetics were studied. According to Everall, the signal in L1 (t1) (Fig. 6) results from a very thin layer below the surface of the DDC membrane. Detectable signals in L1 are mainly present in the region above the reservoir, whereas the layers L2 and L3 (t1) show an increasing drug content also at larger distances from the reservoir. Furthermore, the signal grows with incremental depth, as was expected. Another benefit of depth-resolved chemical imaging is the comparison of sample sections over time. After 60 h (Fig. 6 (t3)) of proceeding drug distribution, signal intensities of the band of dithranol at 616 cm^{-1} in wider regions of the DDC membrane increased in lateral dimension as well as with incremental depth. Indeed, the membrane region, which directly contacts the formulation (L3), shows a decreasing DI concentration with time (Fig. 6). A closer insight into the diffusion process near the formulation/membrane interface is given in Fig. 7a. A part of the membrane, which is located above the reservoir ($x = 3575$; $y = 145–160$), displays decreasing signals in L3 over time, while the intensities in L1 and L2 do not exhibit any similar behaviour. In contrast to this, decreasing signal intensities were first observed in the upper layers 25 h after the beginning of the experiment. Since L3 represents the ointment, we assume these data exhibit the exhaustion of the drug reservoir (ointment). The decelerated transport of DI from the ointment in the membrane and the distribution of DI in the membrane lead after 25 h to decreasing signal intensities of the drug. While the DI penetrates the membrane (partition coefficient 1.37–2.07), the drug in the formulation is prevented from diffusing by the solid fraction of the paraffin. Thus, the process of delivery and diffusion into the membrane is faster than the diffusion of the drug in the viscous ointment. As the diffusion behaviour of the drug in the formulation differs from that in the DDC membrane, a concentration gradient results in the suspension, while the concentration gradient between the membrane and the adjacent suspension decreases. The membrane area around and above the interface has exceeded its maximum drug content after 60 h already. The maximum seems to be reached about 25 h after the start of the experiment. This means that the application of a new unused formulation would be expedient after

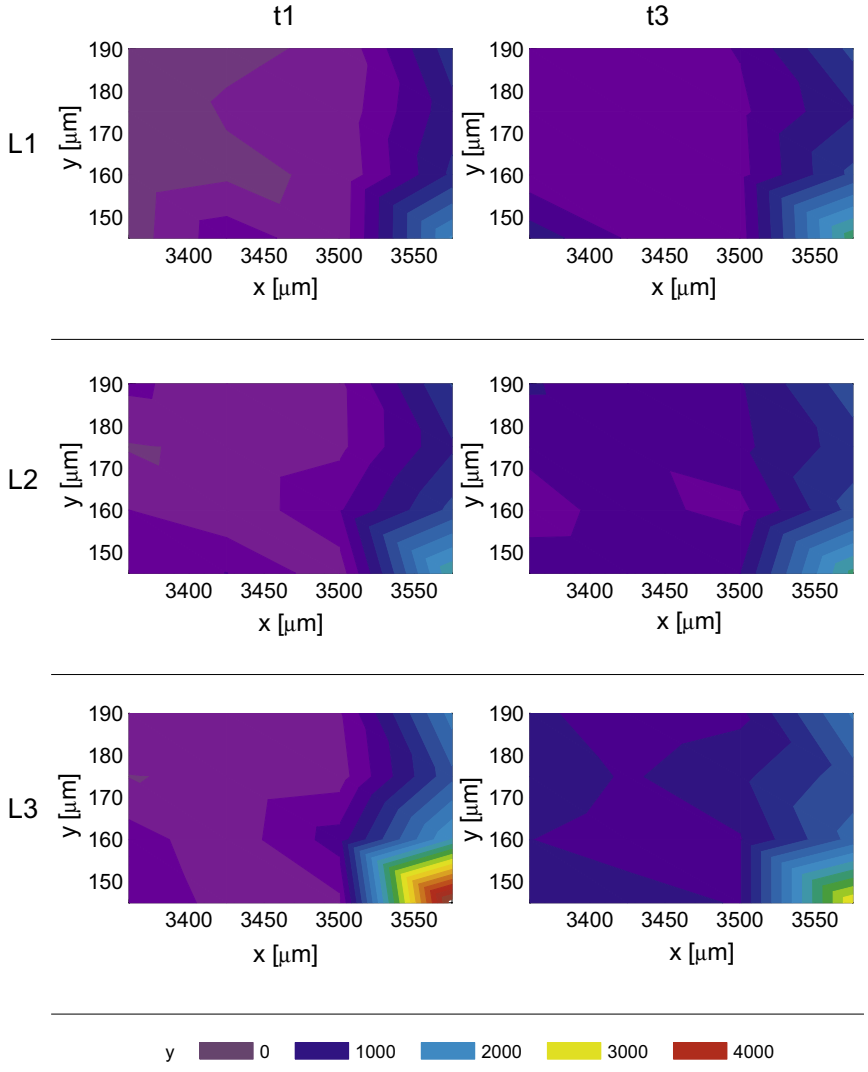

Fig. 6. Chemical images (see Fig. 2) of the DDC membrane (size 45 µm × 215 µm) 15 h (t1) and 60 h (t3) after starting the experiment. t2 is not shown in this figure. Intensity reflects the drug concentration, which is related to the band at 616 cm^{-1}. The mapping measurements were carried out in three depth regions L1 (1.5–2.5 µm), L2 (15–25 µm), and L3 (29–49 µm).

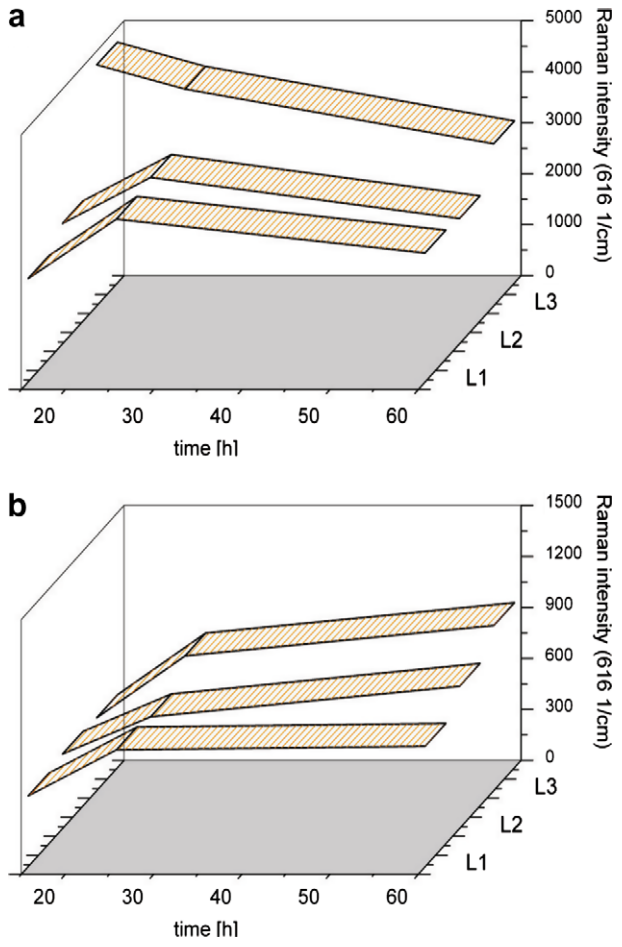

Fig. 7. Dithranol concentration at positions 3575/145 (a) and 3425/160 (b) in the layers L1, L2, and L3 vs. penetration time. In order to extract the drug concentration, the integrated intensity of the dithranol Raman band at 616 cm^{-1} was used.

about one day. For comparison, Fig. 7b displays the same scheme for measurement point (3425/160), which is located 150 μm away from the ointment reservoir. At this position, signals from the drug in all layers are still increasing after 60 h. However, the slope of the function (Fig. 7b) indicates that the velocity of drug enrichment has slowed down. DI is distributed laterally although the concentration levels at distances greater than 75 μm from the reservoir do not reach the values of adjacent membrane regions during the experiment (Fig. 7).

4. Conclusions

Application of series imaging by means of FTIR microscopy and confocal Raman microscopy for studying the delivery of a drug from a semisolid formulation into an artificial membrane was demonstrated successfully. Our results show that the behaviour of dithranol in the observed system is similar to that found by former investigations of Wartewig and Neubert [18]. While the FTIR measurements allow to pursue the lateral distribution of dithranol, CRM additionally offers a 3D follow-up of drug diffusion in the DDC membrane and insight into the donor formulation. Direct FTIR imaging, however, turned out to be unsuitable under the conditions of our investigations. The lower beam intensities in the direct imaging mode, which result from the defocused IR beam, lead to the lower signals.

However, attention must be paid when using CRM: the apparent and true positions of the measuring depth diverge considerably, and these values have to be corrected mathematically. If the composition of a sample changes during the experiment, the spectra from different components overlap, which is another problem. Due to the mapping of multiple layers, the time required by a single Raman measurement (depending on spatial resolution) is longer than that of a comparable IR-Scope measurement. In general, the measurement periods of series imaging experiments depend on the resolution and are rather long. In comparison, the direct imaging mode allows for a faster data acquisition with high lateral resolution. However, concessions have to be made in terms of sensitivity. In order to gain analysable spectra, the FTIR mapping measurements are often carried out in the transmission mode, as the reflection mode produces lower intensities. Consequently, our IR measurements were accomplished in the transmission mode, but this also implied a restricted thickness of the DDC membrane (<15 μm). Otherwise, total absorption of the IR beam was observed. Such limitations did not occur when performing the measurements with the confocal Raman microscope. In conclusion, Raman microspectroscopy seems to be an adequate technology for skin model and skin penetration and drug delivery studies. CRM combines robustness with a marginal sample preparation for depth-resolved 3D measurements and usability for in vivo experiments. Consequently, this method is a powerful analytical tool in the field of membrane penetration or drug delivery measurements. If the SRS technique will improve detection of traces of drugs in tissue, use of Raman microscopy for 3D skin penetration measurements will increase rapidly.

Acknowledgements

The authors thank Stefan Heissler for his very helpful technical assistance in confocal Raman microscopy and Dr. Hendrik Metz for supporting discussions.

References

[1] B.D. Hanh, R.H.H. Neubert, S. Wartewig, Investigation of drug release from suspension using FTIR-ATR technique: part I. Determination of effective diffusion coefficient of drugs, International Journal of Pharmaceutics 204 (1–2) (2000) 145–150.
[2] M. Hartmann, B.D. Hanh, H. Podhaisky, J. Wensch, J. Bodzenta, S. Wartewig, R.H.H. Neubert, A new FTIR-ATR cell for drug diffusion studies, Analyst 129 (10) (2004) 902–905.
[3] B.D. Hanh, R.H.H. Neubert, S. Wartewig, J. Lasch, Penetration of compounds through human stratum corneum as studied by Fourier transform infrared photoacoustic spectroscopy, Journal of Controlled Release 70 (3) (2001) 393–398.
[4] J.M. Chalmers, P.R. Griffiths, Sampling techniques, in: J.M.C.D.E. Pivonka, P.R. Griffiths (Eds.), Applications of Vibrational Spectroscopy in Pharmaceutical Research and Development, Wiley & Sons, 2007, pp. 19–49.
[5] S. Wartewig, R. Neubert, W. Rettig, K. Hesse, Structure of stratum corneum lipids characterized by FT-Raman spectroscopy and DSC. IV. Mixtures of ceramides and oleic acid, Chemistry and Physics of Lipids 91 (2) (1998) 145–152.
[6] N.M. Sijtsema, S.D. Wouters, C.J. De Grauw, C. Otto, J. Greve, Confocal direct imaging Raman microscope: design and applications in biology, Applied Spectroscopy 52 (3) (1998) 348–355.
[7] C. Krafft, T. Knetschke, A. Siegner, R.H.W. Funk, R. Salzer, Mapping of single cells by near infrared Raman microspectroscopy, Vibrational Spectroscopy 32 (1) (2003) 75–83.
[8] N. Uzunbajakava, A. Lenferink, Y. Kraan, B. Willekens, G. Vrensen, J. Greve, C. Otto, Nonresonant Raman imaging of protein distribution in single human cells, Biopolymers 72 (1) (2003) 1–9.
[9] J.J. Andrew, M.A. Browne, I.E. Clark, T.M. Hancewicz, A.J. Millichope, Raman imaging of emulsion systems, Applied Spectroscopy 52 (6) (1998) 790–796.
[10] P.D.A. Pudney, M. Melot, P.J. Caspers, A. van der Pol, G.J. Puppels, An in vivo confocal Raman study of the delivery of trans-retinol to the skin, Applied Spectroscopy 61 (8) (2007) 804–811.
[11] A. Tfayli, O. Piot, F. Pitre, M. Manfait, Follow-up of drug permeation through excised human skin with confocal Raman microspectroscopy, European Biophysics Journal with Biophysics Letters 36 (8) (2007) 1049–1058.
[12] L. Chrit, P. Bastien, G.D. Sockalingum, D. Batisse, F. Leroy, M. Manfait, C. Hadjur, An in vivo randomized study of human skin moisturization by a new confocal Raman fiber-optic microprobe: assessment of a glycerol-based hydration cream, Skin Pharmacology and Physiology 19 (4) (2006) 207–215.

[13] L. Chrit, P. Bastien, B. Biatry, J.T. Simonnet, A. Potter, A.M. Minondo, F. Flament, R. Bazin, G.D. Sockalingum, F. Leroy, M. Manfait, C. Hadjur, In vitro and in vivo confocal Raman study of human skin hydration: assessment of a new moisturizing agent, pMPC, Biopolymers 85 (4) (2007) 359–369.
[14] C.L. Evans, X.S. Xie, Coherent anti-stokes Raman scattering microscopy: chemical imaging for biology and medicine, Annual Review of Analalytical Chemistry (2008) 883–909.
[15] C.W. Freudiger, W. Min, B.G. Saar, S. Lu, G.R. Holtom, C.W. He, J.C. Tsai, J.X. Kang, X.S. Xie, Label-free biomedical imaging with high sensitivity by stimulated Raman scattering microscopy, Science 322 (5909) (2008) 1857–1861.
[16] C.A. Coutts-Lendon, N.A. Wright, E.V. Mieso, J.L. Koenig, The use of FT-IR imaging as an analytical tool for the characterization of drug delivery systems, Journal of Controlled Release 93 (3) (2003) 223–248.
[17] S.G. Kazarian, K.L.A. Chan, Chemical photography of drug release, Macromolecules 36 (26) (2003) 9866–9872.
[18] S. Wartewig, R.H.H. Neubert, Pharmaceutical applications of Mid-IR and Raman spectroscopy, Advanced Drug Delivery Reviews 57 (8) (2005) 1144–1170.
[19] A.G. Bell, On the production and reproduction of sound by light, American Journal of Sciences 20 (1880) 305–324.
[20] H.U. Gremlich, B. Yan, in: H.U. Gremlich, B. Yan (Eds.), Infrared and Raman Spectroscopy of Biological Materials, vol. 24, Marcel Dekker, Inc., New York, 2001, p. 581.
[21] D.E. Pivonka, J.M. Chalmers, P.R. Griffiths (Eds.), Applications of Vibrational Spectroscopy in Pharmaceutical Research and Development, Wiley & Sons, 2007, p. 372.
[22] F. Siebert, P. Hildebrandt, Vibrational Spectroscopy in Life Science, Wiley-VHC Verlag & Co., Weinheim, 2008. p. 310.
[23] H. Günzler, H.U. Gremlich, IR-Spectroscopies, third ed., Wiley-VHC Verlag GmbH & Co, Weinheim, 2003. p. 352.
[24] C.V. Raman, K.S. Krishnan, A new kind of secondary radiation, Nature 121 (1928) 501–502.
[25] G.D.E. Smith, Modern Raman Spectroscopy – A Practical Approach, Wiley & Sons, Chichester, 2005. p. 210.
[26] I.R. Lewis, H.G.M. Edwards (Eds.), Handbook of Raman Spectroscopy, vol. 28, Marcel Dekker Inc., 2001, p. 1054.
[27] H.H. Mantsch, L.P. Choo-Smith, R.A. Shaw, Vibrational spectroscopy and medicine: an alliance in the making, Vibrational Spectroscopy 30 (1) (2002) 31–41.
[28] I.W. Levin, R. Bhargava, Fourier transform infrared vibrational spectroscopic imaging: integrating microscopy and molecular recognition, Annual Review of Physical Chemistry 56 (2005) 429–474.
[29] J. Barbillat, Raman microscopy – developments and applications, in: J.C.G. Turrell (Ed.), Raman Imaging, Elsevier Academic Press, 1996.
[30] A. Christ, J. Szurkowski, B.D. Hanh, S. Wartewig, M. Kopycinska, R.H.H. Neubert, U. Cobet, Drug penetration into a membrane investigated by photoacoustic and FTIR-ATR spectroscopy, Analytical Sciences 17 (2001) S371–S373.
[31] B. Gotter, W. Faubel, R.H.H. Neubert, Optical methods for measurements of skin penetration, Skin Pharmacology and Physiology 21 (3) (2008) 156–165.
[32] B.D. Hanh, R.H.H. Neubert, S. Wartewig, A. Christ, C. Hentzsch, Drug penetration as studied by noninvasive methods: Fourier transform infrared-attenuated total reflection, Fourier transform infrared, and ultraviolet photoacoustic spectroscopy, Journal of Pharmaceutical Sciences 89 (9) (2000) 1106–1113.
[33] B.D. Hanh, Anwendung von nicht-invasiven spektroskopischen Methoden zur Optimierung der Wirkstoffpenetration aus Suspensionen, Doctoral Thesis, Halle-Wittenberg (2001) 47–50.
[34] D. Lin-Vien, N.B. Colthup, W.G. Fateley, J.G. Grasselli, The Handbook of Infrared and Raman Characteristic Frequencies of Organic Molecules, first ed., Academic Press, San Diego, 1991. p. 503.
[35] N.J. Everall, Modeling and measuring the effect of refraction on the depth resolution of confocal Raman microscopy, Applied Spectroscopy 54 (6) (2000) 773–782.